IChemE

www.ingentaselect.com=titles=02638762.htm

0263–8762/03/$23.50+0.00
Institution of Chemical Engineers
Trans IChemE, Vol 81, Part A, September 2003

EXPERIMENTAL STUDY OF A BUOYANT PARTICLE DISPERSION IN PIPE FLOW

Y. LE GUER[1], P. REGHEM[1], I. PETIT[2] and B. STUTZ[3]

[1]Laboratoire de Thermique Energétique et Procédés (LaTEP—EA 1932), Université de Pau et des Pays de l'Adour, Pau, France
[2]Laboratoire de Génie des Procédés, Environnement, Agroalimentaire (GEPEA UMR 6144), Nantes, France
[3]CETHIL, INSA de Lyon (UMR 5008), Villeurbanne, France

An experimental investigation of a solid–liquid dispersion pipe flow was conducted using a pulsed ultrasonic Doppler velocimeter. The solid phase was composed of buoyant particles dispersed in water. This particular two-phase flow was used to mimic the behaviour of ice–water flow. Four diagnostics were used to study the complex nature of the two-phase flow mixtures: mean velocity profiles, space-time diagrams, probability density functions (PDF) and cumulative probability distribution functions (CPDF) of velocities. The results allow detection of the different flow patterns with moving bed, sliding and saltation regimes. Visualizations of the flow supplement the velocity measurements.

Keywords: solid–liquid dispersion; buoyant particles; Doppler ultrasound velocimetry; flow patterns; boundary layer; saltation.

INTRODUCTION

Solid–liquid dispersions are widely encountered in many industrial processes, especially in chemical engineering (thermal energy transportation, process plant transfer pipelines, catalytic reactors, fluidized beds, etc.). Different cases may be distinguished, according to many factors such as: particle type (colloidal or not), monodisperse or polydisperse particle distributions, particle concentrations, density higher or lower than that of the carrier fluid, viscosity of the liquid, laminar or turbulent flow regime (Shook and Roco, 1991). The flow patterns associated give rise to highly heterogeneous flows for which the study is far from complete. The substantial lack of experimental data does not facilitate the elaboration of models to predict flow patterns or pressure drops. Satisfactory modelling involves correct predictions of solid–liquid (particle–fluid or wall–fluid) and solid–solid (particle–particle or wall–particle) interactions in the flow mixture. The turbulence characteristics are then modified by the presence of the particles. Solid–liquid mixture flows also need to be well understood to evaluate forces that become important when high slip occurs: Basset, Magnus, lift and added-mass forces.

Some authors, such as Turian and Hsu (1987), give experimental correlations for slurry flow pressure drops or critical velocity [i.e. limiting deposit velocity (Turian and Hsu, 1987); for an extensive review, see Doron and Barnea (1995)].

The continuum-kinetic theories developed by Wang and Ni (1991) for two-phase flows are only valid for dilute solid–liquid dispersions. A three-layer model was developed by Doron and Barnea (1993) from careful experimental observations of solid–liquid mixtures at low flow rates. This model can predict the existence of a stationary bed, the limit deposit velocity and the transition to fully suspended flow. It was validated for several experimental slurry flows (Doron and Barnea, 1995). Recently, the role of the interface layer in stratified slurry flow was highlighted by Pugh and Wilson (1999) and an anomalous friction mechanism (substantially lower than predicted) was established by Schaan and Shook (2000) for high-velocity slurry flows at high solid concentration.

We present here an experimental study of a buoyant particle dispersion flow. This two-phase fluid model is used to mimic the hydrodynamic behaviour of ice-slurry flow. Because of environmental constraints, ice-slurry flows tend to be used extensively as heat exchange fluid instead of classical CFC and HCFC fluids (Inaba, 2000). This work is motivated first by the need to better understand this particular two-phase flow for various low solid mass fractions. Most of the literature presented until now in the subject has concerned settling dispersion. The influence of inertia and gravity on particles in inducing different flow patterns than those encountered for settling dispersions was also investigated (Doron and Barnea, 1996).

In the following sections we present successively the particles and fluid, the test loop, the pulsed ultrasonic Doppler velocimetry and visualization techniques used to characterize the buoyant dispersion pipe flow. The experimental results are then presented and discussed.

EXPERIMENTAL PARAMETERS AND MEASUREMENT TECHNIQUES

Particles and Fluid

The water continuous phase was laden with non-colloidal prolate–spheroid solid polypropylene particles (translucent

PP granules manufactured by ATOFINA). These particles had a density of 0.889 0.01 which is close to the density of ice (0.917). For precise determination of the density, the particles were suspended in a mixture of water and ethanol. Owing to the differential density with water, buoyancy effects on the particles are important. The mean PP sizes measured for a sample of one hundred particles were 4.3 3.5 3.1 mm. The non-sphericity of particles may be important for the ice-particle similitude (Sari and Egolf, 2001). By filling the complete volume of the loop with PP particles and interstitial water, we estimated the maximum packing volume fraction f_m at 66 1.5%. The solid mass fraction f of the flow was calculated with regard to the maximum volume fraction f_m. Four mass fractions (5, 10, 15 and 20%) were studied here.

The Test Loop

The experimental set-up was a horizontal closed loop made from four glass straight pipes and four 90 glass bends. The inner circular pipe diameter D was equal to 40 mm. The circulation length along the centre line of the loop was 5.395 m and the volume of the loop was equal to 6.65 10^{-3} m^3. A sketch of the loop is shown in Figure 1. A two-blade pitched (45) paddle marine impeller of 35 mm diameter (d) was used to generate the axial flow. The impeller speed N varied from 200 to 2000 rpm. Owing to the large heat exchange area, the temperature elevation of the fluid was limited. The flow in the loop was composed of a high shear region in the vinicity of the impeller (A), a swirling flow region in the straight pipe downstream of the impeller (B), a two-cell helical flow in each bend (BF) and a straight pipe flow region (C). For velocity measurements, the ultrasonic probe was positioned at the end of the long straight pipe (C; Figures 1 and 2) in order to avoid perturbations induced by curved pipe flow. The main experimental parameters are summarized in Table 1.

Ultrasonic Velocity Measurement Profiles

Pulsed ultrasonic doppler velocimetry (UDV; DOP1000[1] Signal Processing, Lausanne) was used to investigate the flow. This new non-intrusive technique presents several advantages over more traditional pointwise velocimetry techniques [laser doppler velocimetry (LDV) or hot wire velocimetry], such as use in opaque flow and to give instantaneous velocity profiles of the flow. This last property is particularly interesting to study unsteady (transient, pulsating or oscillating) and turbulent flows. With the LDV technique, the solid–liquid flow needs to be sufficiently transparent to scattered emitting laser light. For high solid concentrations, the light is absorbed before reaching the probe detector. In some case a refractive index matching technique can be used to overcome the problem of limited concentration. Also, for LDV, a focusing problem of the laser beams can occur when curved dioptres are encountered (flows in pipe or bends).

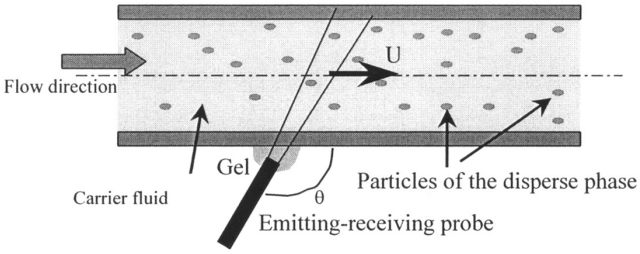

Figure 2. Experimental arrangement of the UDV.

In this context, the UDV presented in our experimental study is a new and alternative promising investigation technique for slurry flows. This technique is based on the measurement of the time lapse between the transmission of ultrasonic bursts and the reception of echoes generated by particles flowing in the liquid, giving the position of the scattering volumes. By measuring the Doppler frequency shifts of these particles a velocity profile is obtained after few ultrasonic emissions. The particle velocity U can be calculated from the measured Doppler shift f_D, using the relation:

$$U = \frac{c \, f_D}{2 \, f_e \, \cos y}$$

Iriodine[1] flakes with mean dimensions of 10–20 mm were used as reflecting particles for the water continuous phase. Iriodine is a special class of pigment produced by Merck,

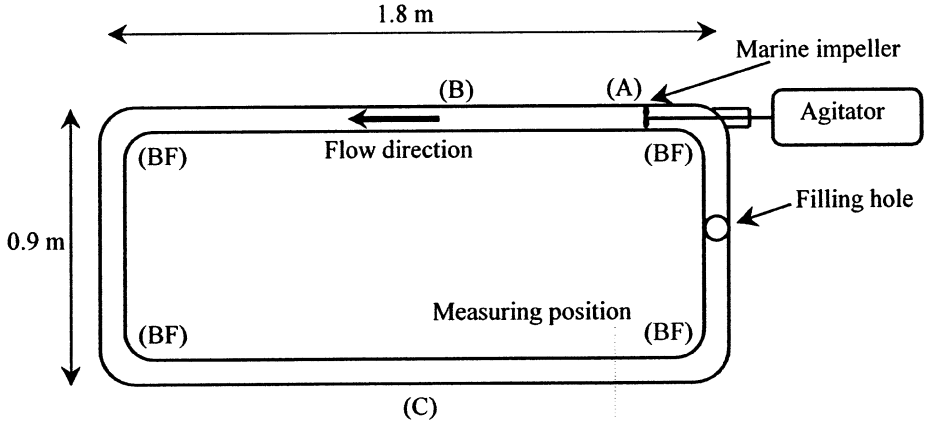

Figure 1. Experimental recirculating flow loop: (A) high shear region; (B) swirling flow region; (BF) two-cells helical flow region; (C) straight pipe flow region.

Table 1. Experimental parameters.

Materials	
Particle	PP, polypropylene
Carrier fluid	Water
Particle properties	
Density r_p	0.889 0.01 g cm ^{3}
Mean dimensions	4.3 3.5 3.1 mm^{3}
Operating conditions	
Impeller speed	20–200 s ^{1}
Particle mass fraction, f	0–20%

with pearl gloss obtained by adding oxides of various metals. They were added at a 0.03% concentration by weight. They also allow a visual observation of flow structures around PP particles. The ultrasonic transducer was affixed to the outer surface of the glass pipe, making an angle y with the pipe axis. The diameter of the ultrasonic beam was 5 mm. This setup measured the velocity profile of the axial velocity component $U_x(x;t)$ along the ultrasonic propagating direction from the lower pipe wall to the upper one. The measuring volume had a half-disc with a radius of 2.5 mm and a thickness 0.375 mm. As an example this setup required a measuring time of 38 ms for each profile corresponding to 128 ultrasonic emissions. This measuring time can vary depending on the choice of the number of emissions. A total of 1000 profiles were recorded in the memory of the instrument and then transferred for later analysis. The specifications of the UVP in our experimental configuration are summarized in Table 2.

This UDV technique was used by Antoine and Lebouché (1998) to study a non-Newtonian suspension in pipe flow. One may find further details on this technique in Takeda (1991, 1995), who developed the UDV. His work proved for different experiments that accuracies of 5 and 1% are obtained, respectively, for velocity and position. The UDV is also very efficient in collecting spatiotemporal mappings of the flow.

Visualization of the Flow Mixture

Flow visualization is accomplished by capturing patterns of the flow issued from a CCD camera. Images were digitized by a colour video frame grabber (Scion CG-7 RGB Color) directly from the video camera. They also could be stored on a SVHS video recorder to be seen later on a monitor. Some of the PP particles were coloured so they could be followed individually along their trajectory. An attempt was made to use the laser-induced fluorescent (LIF) sheet flow visualization technique, but the results were not conclusive for an effective illustration of the flow.

Table 2. Specification of the UDV in our experimental configuration.

Emission frequency	8.0 MHz
Repetition in a pulse	8 cycles
Pulse repetition frequency	<208 ms
Number of emission=profile	128 (32 ms)
Resolution	0.375 mm
Sound speed	1491 m s ^{1}
Doppler angle	70

EXPERIMENTAL RESULTS AND ANALYSES

Flow Patterns

Experiments were performed with four mass fractions of the dispersed phase (5, 10, 15 and 20%). For each experiment the flow was studied for different rotational impeller speeds (1000, 1200, 1500, 1700 and 2000 rpm). The definition of a Reynolds number requires the choice of an effective viscosity for the mixture. This is not trivial when the solid–liquid flow is highly heterogeneous. The definition of a bulk viscosity for low or medium dilute dispersion constitutes the subject of active research (Coussot and Ancey, 1999).

As for the flow of particles denser than the carrying fluid (Turian and Yuan, 1977; Doron and Barnea, 1996), three main flow patterns ranging from low to high velocities of the continuous phase have been observed:

(1) Flow with stationary bed—when the velocity of the continuous phase is low, all the particles rise immediately to the top of the pipe and remain fixed with regard to this surface. The equilibrium of this stationary bed implies a fluid–solid coupling: the shear stresses near the wall are not adequate for setting in flow the network of particles. These stresses depend on the varying pressure within the interstitial fluid.

(2) Flow with a moving bed—for this flow, we can distinguish two particular cases: (a) a clustered moving bed for which the convective velocity of particle clusters is different from the continuous phase velocity. The saltation mechanism governs the flowing of a cluster. Particles located upstream of a cluster subjected to a strong velocity gradient are entrained under the particle bed where the velocity of the carrier fluid is high. As soon as the end of the cluster is reached, these particles rise very quickly under the influence of buoyancy. Then they follow the wall until they reach again the frontal position of the cluster. Thus the cycle is repeated. Some particles also move by successive bounces on lateral particles of the bed; (b) a continuous bed. When the continuous phase velocity increases or when the mass fraction of the disperse phase is higher, clusters tend to spread out and the bed becomes continuous along the loop.

(3) Fully suspended flow (not observed with this loop). The fully suspended flow regime (or pseudo-homogeneous flow) occuring when all the particles are supported by the fluid was not observed in our experimental conditions. This was due to the maximum rotational speed of the impeller, which was limited to 2000 rpm. It was, however, observed for the flow developed in another test rig in our laboratory for exactly the same type of two-phase mixture (Reghem, 2002).

Figure 3(a)–(c) gives photographs of the three flow patterns observed for the buoyant dispersion studied at the higher solid mass fraction.

Velocity Profiles

In Figure 4 a typical spatiotemporal evolution of the axial velocity profiles component for an impeller speed

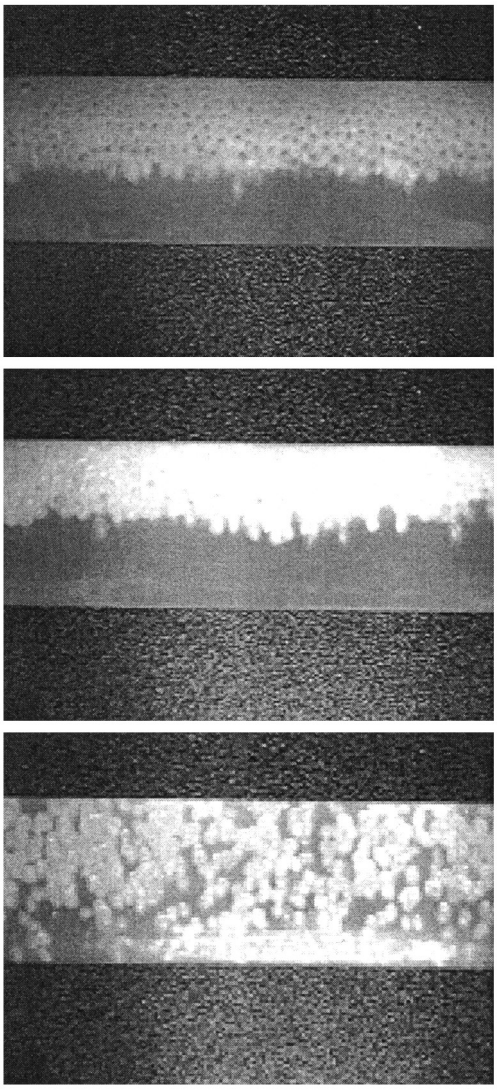

Figure 3. Photographs of the solid–liquid buoyant flow for the three flow regimes at the higher solid mass fraction: (a) stationary bed; (b) moving bed; (c) fully suspended flow.

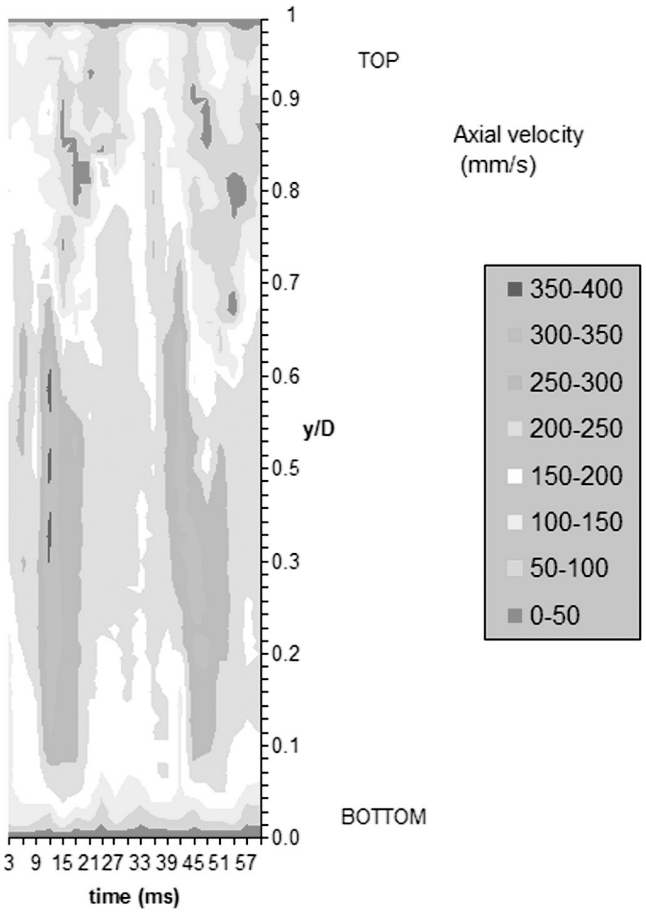

Figure 4. Space–time diagram of the axial velocity component for an impeller speed of 1200 rpm and f ¼ 5%.

of 1200 rpm and a mass fraction of 5% is shown. The flow associated with this regime is the clustered moving bed flow. In this plot all the velocity profiles are presented vertically. A particle cluster corresponds to the low velocities observed along the top of the pipe. The flow of two clusters appears clearly (on the upper plot), and nearly 30 s separate their arrival. Correspondingly, under a particle cluster an increase of the axial velocity with a shift of its maximum towards the bottom of the pipe can be observed. After the cluster transit, the axial velocity profile becomes more symmetric, as observed in a flow without particles.

In order to investigate the buoyant particle dispersion, axial velocity profiles were performed at five impeller speed rotations (1000, 1200, 1500, 1700 and 2000 rpm) for different mass fractions of the dispersed phase, f ¼ 0, 5, 10, 15 and 20%. Only the mean axial velocity profiles for an impeller speed of 1200 rpm are presented in Figure 5. The same features were observed for the flow regimes from 1000 to 1700 rpm. At 2000 rpm the results were not so similar to the previous ones, and some of them seem to be overestimated. This is probably due to a unsatisfactory determination of the Doppler angle y.

The flow regime studied at f ¼ 0% corresponds to the transitional flow regime between a laminar flow and a turbulent one. All the velocities are indicated in dimensional quantities. From f ¼ 5% to f ¼ 20% the transformation of the velocity profile due to the presence of the solid phase can be seen. At low mass fractions, f ¼ 5% and f ¼ 10%, the thickness of the solid bed flowing on the top of the pipe cannot be evaluated, mainly due to the fact that for these experiments, as seen before, the bed was not continuous along the loop.

For the highest mass fraction, f ¼ 15% and f ¼ 20%, the mean velocities on the upper part of the pipe were reduced towards a value which corresponded, at the pipe boundary, to the steady velocity of the bed observed. Correlatively the maximum of velocity was shifted towards the bottom wall and was always located under the pipe axis, as explained for the spatiotemporal velocities plot (Figure 4).

For low rotational speeds, the bed seemed to play the role of a porous material, this was confirmed by the variation in the slope observed in the velocity profile at the lower part of the bed; a boundary layer was developing between the bed and the liquid phase. For the lowest rotational speed (1000 rpm), under the bed, a nearly parabolic profile was observed. This discontinuity was less pronounced at higher flow rates, for which dragging of particles by sliding, rolling, saltation and turbulent dispersion acted more on the flow.

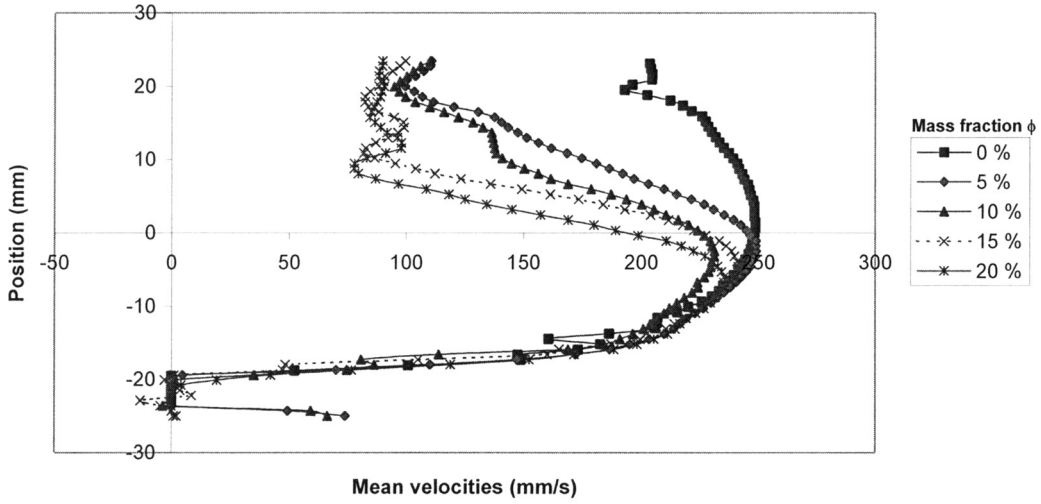

Figure 5. Mean axial velocity profiles for different mass fractions f of the dispersed phase and for an impeller speed of 1200 rpm.

For high mass fractions (f ¼ 15% and f ¼ 20%), the visualization of the flow patterns showed the existence of a well-defined moving bed. The bed had a thickness of approximately 30% of the pipe diameter (12% of the pipe cross section) and did not vary significantly for the different rotational speeds. Its velocity was also nearly constant for low and medium flow rates (80–90 mm s ^{1}), but was twice this value for the highest flow rate (200 mm s ^{1}).

We observed that the boundary layer under the bed (except for 1000 rpm) presented a zone of constant shear very well characterized by a linear slope over a quarter of the pipe diameter. For each flow rate, the value of the shear rate was conserved for the velocity profiles corresponding to f ¼ 15% and f ¼ 20%. The slope was the same, the thickness of the bed was just more important for f ¼ 20%, leading to a shift of the maximum velocity towards the bottom wall of the pipe.

As can be seen for velocity profiles on Figure 5, a major drawback of the UDV technique is the difficulty of eliminating endwall effects and scattering across imiscible phase interfaces. As an example, for f ¼ 0% (Figure 5), the multiple reflections of the ultrasonic waves at the top pipe wall transformed this interface to a transmitter and as a result gave imaginary velocity values outside the region of the flowing dispersion. Consequently, the zero expected value of the velocity at the pipe wall was not obtained.

Statistical Analysis

Since the instantaneous measurements of velocity profiles were in a vector form, their statistical treatment was possible in order to extract some characteristics of the flow. The statistical analysis tools chosen for this study are the probability density function (PDF) and the cumulative probability distribution function (CPDF). The PDF is a function of the velocity signal amplitude and a measure of the probability that the signal will have a certain range of values. If the range of velocity fluctuations of a signal is divided into equal increments, DU, and the number of data samples occurring in an increment is divided by the total number of data samples, the result is the probability P_j that the velocity of an individual data point will be in that range of velocity. The cumulative probability density, C_j, is the probability that a velocity will occur in the first jth increments, and is given by:

$$C_j = P_1 + P_2 + \cdots + P_j$$

Both functions, PDF and CPDF reveal information about velocity fluctuations on a particular measurement location along the ultrasonic beam (i.e. at different transverse depth positions). Figures 6 and 7 are associated with flow regimes with a rotational impeller speed of 1200 rpm. The PDF of Figure 6(a) is given for a pure water flow (without PP particles). It shows a Gaussian distribution of velocities for all the transverse positions. The maximum peak velocity of distributions is effectively observed for the pipe axis position. This Gaussian distribution also indicates that the seed particles (Iriodine flakes) follow the liquid phase very closely.

In Figure 6(b) is shown the PDF of the flow case which corresponds to the presence of a moving bed with particle clusters. This phenomenon is clearly illustrated by the bimodal distributions of velocities. As shown for the spatio-temporal plot in Figure 4 for the same flow case, the velocity of the carrier fluid is largely affected by the flowing of a particles cluster. The Gaussian distribution observed for the 25 mm depth indicates that in this flow region the passage of the particle cluster does not produce important modification of the mean velocity. From this position, moving up along the vertical diameter towards the top pipe wall, the lower velocities peak corresponds to the flowing of a particle cluster and the higher one to the velocities when only the carrier fluid is present. However, moving down towards the bottom pipe wall the phenomenon is inverted, the higher velocity peak corresponds, this time, to the flowing of a particle cluster. Figures 6(c) and 7 are two different representations of the same results for the maximum mass fraction of the disperse phase (20%). The flow regime observed is a moving continuous bed. The PDFs again find Gaussian shapes as for f ¼ 0%, but present significant spreading when velocities are measured in the particle bed. The maximum of velocities are obtained under the bed for 10 and 15 mm depths. This is confirmed on the CPDF

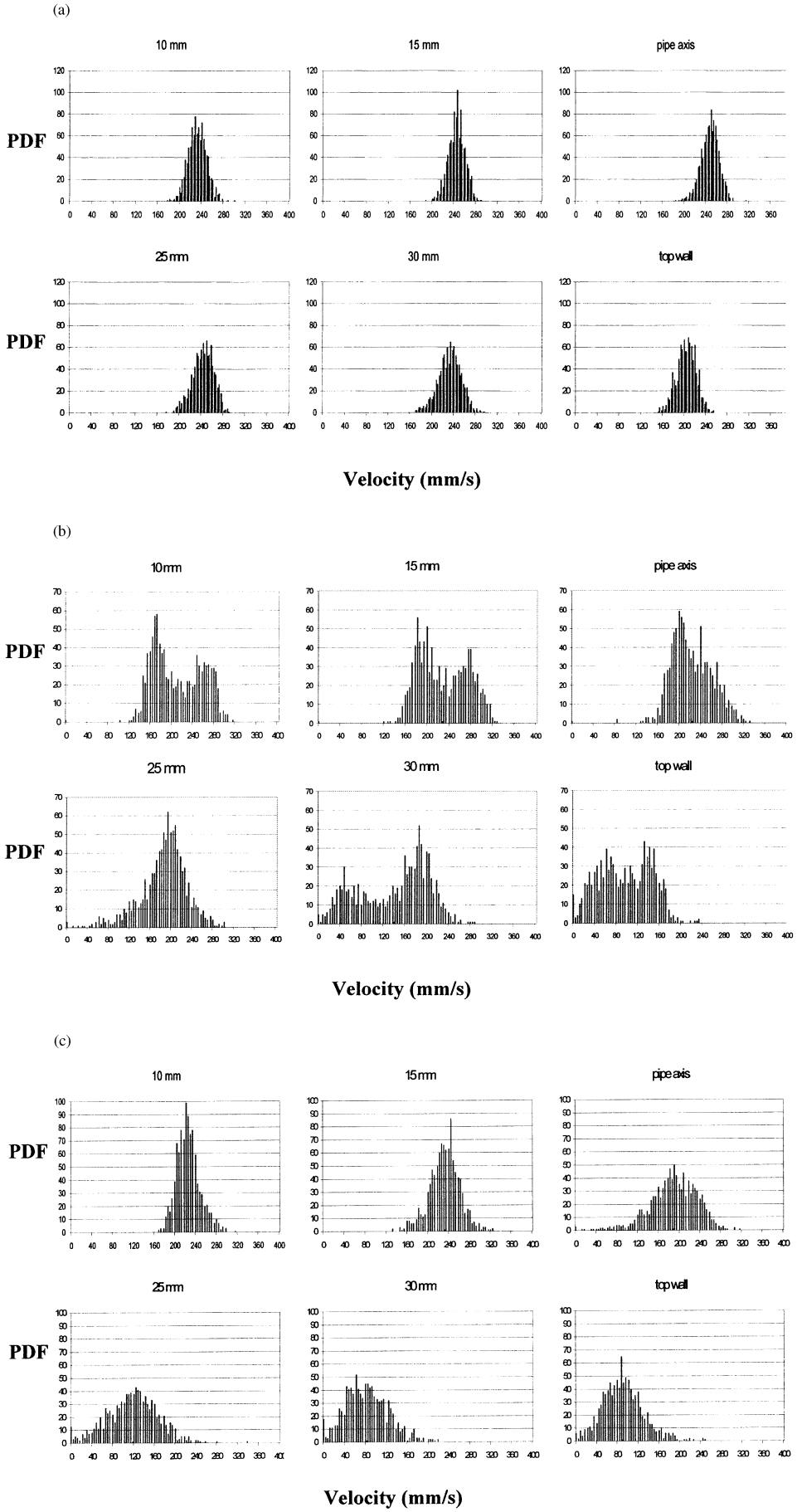

Figure 6. Probability density function (PDF × 1000) on velocities for an impeller speed of 1200 rpm. (a) f = 0%; (b) f = 10%; (c) f = 20%.

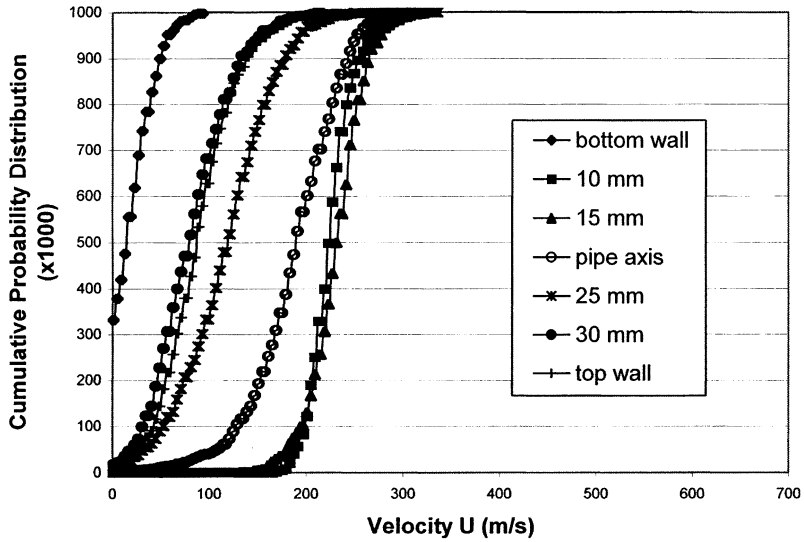

Figure 7. Cumulative probability distribution function (CPDF □ 1000) on velocities for an impeller speed of 1200 rpm and f ¼ 20%.

representation. For 30 mm and top wall measurement locations, the maximum of velocities is centered about a value of 80 mm s ^{1}, which seems to be the convective velocity of the particle bed (the same value appears also in Figure 5 for mean velocities near the top wall). The CPDF plot shows clearly the disymmetry of the velocity distributions with respect to those obtained for the pipe axis. The two distributions corresponding to measurements on the particle bed are very close and indicate also a nearly uniform velocity of the particle bed.

CONCLUSION

The aim of the present experimental investigation was to study the flow patterns encountered for a buoyant dispersion in water. This work demonstrates the potentiality of the UDV technique for flow pattern recognition despite measurement difficulties. The effect of varying mass fraction on velocity profiles has been examined. From the results obtained in the course of the present work, the following can be concluded:

(1) Different flow regimes already known for settling dispersion flows have been identified (stationary bed, moving bed with and without particles cluster and fully suspended flow).
(2) The observation of the velocity profile deformation when a cluster flows can give, as time evolves, the repartition of the solid fraction in a section of the pipe.
(3) For continuous moving bed flow regimes, a constant shear zone under the bed for different mass fractions has been identified. Also small velocity gradients exist inside the bed, indicating a relatively uniform convective velocity of the bed over its height.
(4) The discrimination between solid and liquid velocities (sliding), as reported by Chen and Kadambi (1995) for LDV measurements in a settling slurry flow, was not highlighted in our experiments. The bimodal distribution corresponds here to an intermittent flow with successive periods of high and low velocities due to the presence of particle clusters.

Finally, the full prediction of buoyant dispersion pipe flows is a challenging three-dimensional flow problem that requires further investigation.

NOMENCLATURE

c	sound velocity on the carrier fluid, m s$^{\square 1}$
C_j	cumulative probability density
d	impeller diameter, m
D	internal pipe diameter, m
f_e	emission frequency, Hz
N	impeller speed in revolutions per minute, rpm
P_j	probability
U	UDV measured velocity, m s$^{\square 1}$
x	axial position along the pipe, m

Greek symbols

f	solid mass fraction
f_m	maximum packing fraction
DU	velocity increment, m s$^{\square 1}$
y	Doppler angle, □

REFERENCES

Antoine, Y. and Lebouché, M., 1998, Détermination des vitesses de glissement lors de l'écoulement d'une suspension non-newtonienne par utilisation de la vélocimétrie ultrasonore à effet Doppler, C R Acad Sci Paris, 326(Série IIb): 367–372.

Chen, R.C. and Kadambi, J.R., 1995, Discrimination between solid and liquid velocities in slurry flow using laser Doppler velocimeter, Powder Technol, 85: 127–134.

Coussot, P. and Ancey, C., 1999, Rheophysical classification of concentrated suspensions and granular pastes, Phys Rev E, 59(4): 4445–4457.

Doron, P. and Barnea, D., 1993, A three-layer model for solid–liquid flow in horizontal pipes, Int J Multiphas Flow, 19(6): 1029–1043.

Doron, P. and Barnea, D., 1995, Pressure drop and limit deposit velocity for solid–liquid flow in pipes, Chem Eng Sci, 50(10): 1595–1604.

Doron, P. and Barnea, D., 1996, Flow pattern maps for solid–liquid flow in pipes, Int J Multiphase Flow, 22(2): 173–283.

Inaba, H., 2000, New challenge in advanced thermal energy transportation using functionally thermal fluids, Int J Therm Sci, 39: 991–1003.

Pugh, F.J. and Wilson, K.C., 1999, Role of the interface in stratified slurry flow, Powder Technol, 104: 221–226.

Reghem, P., 2002, Etude hydrodynamique de fluides diphasiques solide–liquide en conduite circulaire: application au coulis de glace, Ph.D. Thesis, Université de Pau et des Pays de l'Adour, Pau, France.
Sari, O. and Egolf, P., 2001, Viscosity applied to the Bingham substance ice-slurry, in 2nd Workshop on Ice slurries, Lucern, Switzerland, 16–18 May, pp 68–80.
Schaan, J. and Shook, C.A., 2000, Anomalous friction in slurry flows, Can J Chem Eng, 78: 726–730.
Shook, C.A. and Roco, M.C., 1991, Slurry Flow: Principles and Practice (Butterworth-Heinemann, Boston, MA).
Takeda, Y., 1991, Development of an ultrasound profile monitor, Nucl Eng Des, 126: 277–284.
Takeda, Y., 1995, Velocity profile measurement by ultrasonic Doppler method, Exp Therm Fluid Sci, 10: 444–453.
Turian, R.M. and Yuan, T.F., 1977, Flow of slurries in pipeline, AIChE J, 23(3): 232–243.
Turian, R.M. and Hsu, F.L., 1987, Estimation of the critical velocity in pipeline flow of slurries, Powder Technol, 51: 35–47.
Wang, G.Q. and Ni, J.R., 1991, The kinetic theory for dilute solid–liquid two-phase flow, Int J Multiphase Flow, 17(2): 273–281.

ACKNOWLEDGEMENTS

The authors wish to express their sincere thanks to students A. Gil and D. Helary from ENSGTI Pau for their participation during some experiments. The authors also gratefully acknowledge the financial support of the Conseil Régional d'Aquitaine.

ADDRESS

Correspondence concerning this paper should be addressed to Dr Y. Le Guer, Laboratoire de Thermique Energétique et Procédés (LaTEP—EA 1932), Université de Pau et des Pays de l'Adour, Rue Jules Ferry, 64 000 Pau, France. E-mail: yves.leguer@univ-pau.fr

The paper was presented at the 9th Congress of the French Society of Chemical Engineering held in Saint-Nazaire, France, 9–11 September 2003. The manuscript was received 4 March 2003 and accepted for publication after revision 1 August 2003.